On-chip Spectral Analysis with Low Power and Optimal Control for Energy Harvesting Using Piezoelectric Devices

Gustavo Monte, Damian Marasco
Departamento de Ingeniería Electrónica
Universidad Tecnológica Nacional, FRN
Rotter S/N, Plaza Huincul, Neuquén, Argentina
e-mail: gustavo.monte@ieee.org

Andrés García, Emanuel Perotti
GIMAP (Grupo de Investigación en Mecánica Aplicada)
Universidad Tecnológica Nacional, FRBB
11 de Abril 461, Bahía Blanca, Buenos Aires, Argentina
e-mail: andresgarcia@frbb.utn.edu.ar

Abstract—**This paper presents a low power DC-DC buck-boost topology functioning battery-less on the basis of a novel technique using a combination of both: singular optimal control plus an analog circuit control law. The very low power consumptions along with the optimal energy harvested, makes possible to perform FFT calculations on-line and on-chip for vibration analysis applied to wind-turbines maintenance operation using an ST microcontroller and transmitting up to 500 m. The complete functioning circuit is shown along with real measurements.**

Keywords—Spectral analysis, Microcontroler, Optimal control, Low power, Analog Devices.

I. Introduction

Energy harvesting is an active research area nowadays (see for instance [1], [2] and [3]). However, piezoelectric devices offer a promising developing field for low power applications (see [4]).

Piezoelectric energy harvested ranges from micro-watts to milli-watts when applied to a pure resistive load. Moreover, this small amount of energy harvested can decrease dramatically when used in a real application if not optimized (see [7]).

Accordingly, the internal model of a piezoelectric appears as capacitive-resistive with the obvious need of complex structures to satisfy the well-known maximum power transfer theorem ([7]). On the other hand, besides an optimal output power, a real application of the energy harvested requires a regulated output voltage which can be accomplished using a buck-boost converter (see for instance [8]).

The choice of buck-boost topologies is explained by the fact of behaving as pure resistive input impedances ion average ([8]). As reported in [6], an optimal control technique to drive a buck-boost converter using a low power microcontroller on the basis of Pontryagin's principle is very appealing.

However, in order to completely render the design battery-less, the start-up of the microcontroller as long as the rest of the circuitry must be projected.

In this paper a complete design using a low power microcontroller from Texas Instruments: MSP430G2230 with the innovation of an analog optimal control implementation using OPA333 (low power rail-to-rail operational amplifiers) will be presented.

Moreover, once a complete DC-DC solution is available with a regulated DC voltage from a piezoelectric device, this energy is ready for using in real applications. The focus is on vibration analysis for wind-energy generators using accelerometers ([9] and [10]).

This analysis is executed in a separate microcontroller, which in this paper is an ST microcontroller: Cortex M4 STM32L4 series with a dynamic run mode of 36uA/MHz. The spectral analysis algorithms are optimized on-chip and they are based on the standard IEEE 21451-001-2017.

This paper is organized as follows: Section II presents a review of the internal models of piezoelectric devices available in the literature for the sake of completeness, Section III presents the state space model of a buck-boost whereas Section IV review the optimal control law for the Buck-Boost presented at [6]. Section V presents some experimental measurements for both: optimal control and spectral analysis. Finally, Section VI presents some conclusions and future work.

II. Energy Harvesting Using Piezo Devices

Many electromechanical piezoelectric's models have been considered in the literature (see for instance [11]).

To start, available data in the literature ca be used adjusting to specific piezoelectric devices (see for instance the model in [7] and [11] in Table I and Fig. 1).

TABLE I. SERIE PIEZO-DEVICE'S PARAMETER VALUES AT [7]

Internal Impedance				
$R_0(\Omega)$	$R_1(\Omega)$	$C_0\ (\mu f)$	$C_1\ (mf)$	$L_1(\mu Hy)$
5	115	0.15	0.277	30.253

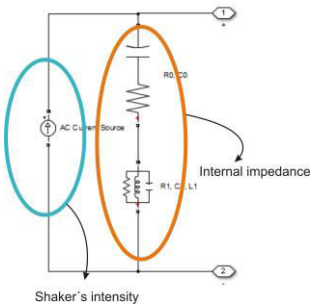

Fig. 1. Piezo-device's internal's electrical model

III. THE BUCK-BOOST TOPOLOGY

As indicated in [8], the Buck-Boost topology is utilized because of its inherent capacity to behave as pure resistive average input impedance.

For the sake of completeness, a review of input impedance behavior is reviewed in this section. The average resistive input impedance is summarized in Table II (see [8]).

TABLE II. BUCK-BOOST AVERAGE INPUT IMPEDANCE

Discontinuous Mode	Continuous Mode
$R_{IN}=2.L/(D^2.T_W)$	$R_{IN}=((1-D)/D)^2.R_L$

Where T_W is the switching's frequency period and R_L the load's resistance.

A. State-Space Model

The state-space model in [6] is reviewed in this section (Fig. 2):

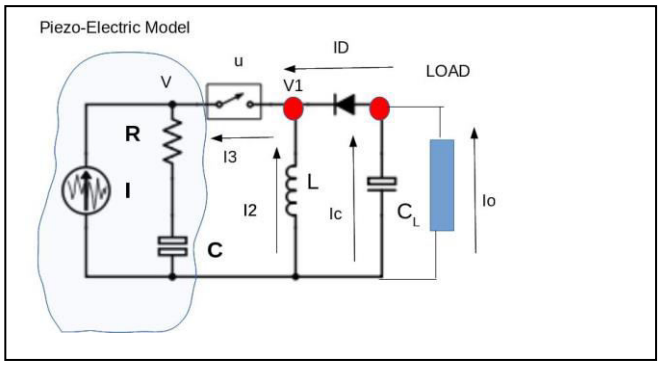

Fig. 2. Buck-Boost topology

Modeling the switch u as: $R^*.u$, with R^* a constant resistance. Equation (1) models the electrical states:

$$\dot{x_1} = \frac{1}{C_L} \cdot [F(\dot{x_2} - x_1) - I_0]$$

$$\dot{x_2} = \varphi_1 \cdot \left(\frac{1 + sign(\varphi_1 - x_1)}{2}\right) + \varphi_2 \cdot \left(\frac{1 + sign(\varphi_2 - x_1)}{2}\right) - (1 + u) \cdot \left(\frac{x_1}{R_D} + \frac{x_2}{L}\right) +$$

$$\varphi_1 = \frac{\frac{u}{R} \cdot (\phi + (x_2 - x_3) \cdot u)}{(1 + u) \cdot \left(\frac{u}{R} - \frac{1}{R_D}\right) + u}$$

$$\varphi_2 = u \cdot R \cdot \left(\frac{-2 \cdot x_2}{L} + \frac{\phi}{R} + \frac{(x_2 - x_3)}{R}\right) + (1 - u) \cdot \left(x_1 + \frac{R_D}{L} \cdot x_2\right)$$

$$\dot{x_3} = \phi(t) + (\dot{x_2} - \dot{x_3}) \cdot u \cdot \left(\frac{R}{R^*}\right) + + \left(\frac{u}{R^* \cdot C}\right) \cdot (x_2 - x_3) \quad (1)$$

Where $\{x_1=dv_0/dt,\ x_2=dv_1/dt,\ x_3=dv/dt\}$, $sign()$, the well-known sign function and $R=R^*$ and $F(.)$ is the current-voltage piecewise linear diode's model (see [6]) More compactly:

$$dx(t)/dt=f(x,u,I_0,\phi),\ \phi=I(t).R+(1/C).\int I(\sigma).d\sigma \quad (2)$$

With $x=[x_1,x_2,x_3]'$ and modeling I_0 as an external perturbation.

IV. LOW POWER OPTIMAL CONTROL STRATEGY

To maximize the output power delivered by the Buck-Boost, an optimal control strategy is needed. Following the singular optimal policy introduced in [6], the general problem leads (see for instance [12]):

$$min_{u \in U}\ \varphi(x(T)) + \int_0^T F(u,t).dt$$

such that: (3)

$$dx/dt=f(x,u,\xi)$$
$$g(x) \leq 0$$

Where U is known as the admissible set, $\xi(t)$ is a possible external perturbation and T is a fixed time (unless $F=1$).
The particular case $F(u,t)=0$, it is known as singular optimal control (see [5]).
In this way, a singular optimal control policy for the model in equation (1) in order to maximize the output power can be posed:

$$min_{u=0,1}\ -x_1(t).I_0(t)$$

such that: (4)

$$dx/dt=f(x,u,\xi)$$

$$(x_1-v_0^*)^2 \leq \Delta v$$

The constraint avoid the trivial solution: $x1(t).I_0(t)=0$, considering Δv as a constant and with v_0* the desired output voltage.

To reformulate (4) in the classical context (3), a new time variable is defined: $\tau \in [0,t]$ along with:

- $(x_1- v_0^*)^2 < \Delta v$
- $(x_1- v_0^*)^2 = \Delta v$

Then, the control law arises:

$$u=(1-sign(I_0.(v_1-v)))/2 \quad (5)$$

A. Stability analysis

The optimal policy obtained in previous section is in fact closed-loop. The stability analysis in [6] can be recovered in this section to give:

- Trajectories with $(x_1- v_0^*)^2 \leq \Delta v$
- Trajectories with $(x_1- v_0^*)^2 > \Delta v$

The first inequality case renders the output voltage bounded:

- v_0=bounded→v_1=bounded(diode)→x_2=bounded (inductance)
- v=bounded(piezoelectric) →$x_3=\int v(\sigma).d\sigma$=bounded

Whereas the state x_3 can be proved to be bounded:

- $u=0 \rightarrow x_3$=finite integral=bounded
- $u=1 \rightarrow x_3$=inductance's

The last equality case above means that the output voltage lies outside the region where the optimal control becomes active. In this case, a fixed pulse width modulation (PWM) renders the system stable.

V. Spectral Analysis On-Chip: Acceleration Information

A. Sampling of sensor signals

Even though uniform sampling is the principal approach used, it doesn't provide a straightforward platform for information and knowledge extraction, it provides only the signal value at a specific instant. *In a signal, the information is embedded in the relationship among samples at different time instants*. Fig. 3 shows a desirable sampling approach in which explicit information is obtained about the signal value at two different time instants.

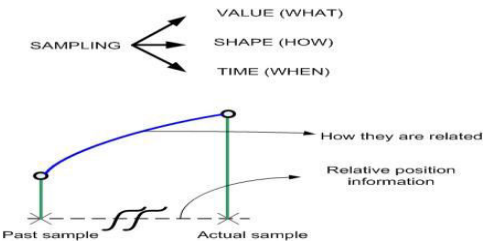

Fig. 3. Uniform sampling provides only the signal value at a particular instant. A more complete description is needed, especially how samples relate each other.

The main idea for representing a sensor signal is to use a concatenation of known function segments instead of samples. The signal information is related directly to the sequence of segments. In [14] a signal is considered that lives in a union of different subspaces. Since the objective is to build a model to extract knowledge in real time, and it must be simple enough to embed it into transducers, a finite set of subspaces represented by simple trajectories is used. In the context of energy harvesting, efficiency implies lower consumption.

The sensor signal is represented by the concatenation of a normalized function that can be dilated, contracted and adapted to follow the real signal in a subspace bounded by an error as shown in Fig. 4. Eight segment classes are enough to approach the real signal. Classes "a", "b" and "c" exist due to a real constrain of the segment length. Class "h" must be avoided by splitting it into different classes.

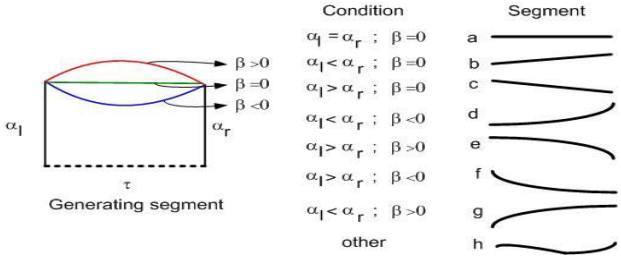

Fig. 4. The generator segment and the eight simplified signal trajectories.

The sensor signal is described by the sequence of values of α,β and τ.

An efficient algorithm is needed for comparing the real signal, suitable for embedding it into transducers, to determine which segment is the best for the real signal segment. In [15] an algorithm was proposed for sensor signal preprocessing. The central idea is to compare real signal trajectory against linear trajectory. Checking how the real departs from linear allows deciding when the simplified segment must end since the error is greater than a prefixed value. This algorithm is described in [16]. It is called **RTSAL** "*Real Time Segmentation and Labeling*". It employs oversampling to check at a rate fast enough, the real signal against simplified trajectories. The algorithm outputs are the values of α, β and τ that represent signal segments. Three vectors, ***Mark*** (α), ***Class*** (β) and ***Time*** (τ), in short **MCT** characterize the digital sensor signal. Fig. 5 shows the segmentation applied to a test signal.

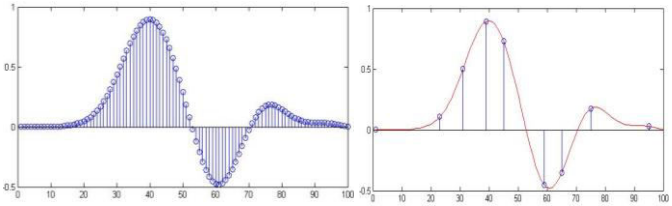

Fig. 5. MCT algorithm applied to test signal. Left: oversampled signal. Right: Tagged samples that delimit only eigth segments.

MCT vectors are the building blocks for this sampling technique. The algorithm uses linear interpolation to track linear trajectories, therefore it is simple an efficient for being executed in real time.

B. Spectral analysis

The spectral analysis using MCT could be more efficient that the FFT for two reasons. First is the application where the analysis is required only at specific frequencies. Second, the samples involved in the spectral calculation are those determined in the MCT sampling process. These two facts may determine that the number of operations required is less than the FFT.

if $x[n]$ is the sensor signal sampled at uniform intervals, the signal from the MCT sampling is:

$$x[n] = x[t_k] * \delta[n - t_k] \tag{6}$$

Where $t_k = t_1, t_2, \dots, t_M$ are the temporal positions of the **M** essential samples. In the frequency domain:

$$X(e^{jw}) = \sum \sum_{k=0}^{M} x[t_k] * \delta[n - t_k] * e^{-jwn} \tag{7}$$

Therefore,

$$X(e^{jw}) = \sum x[t_k] * e^{-jwt_k} \qquad t_k = t_1, t_2, \dots, t_M \tag{8}$$

Where w is the continuous angular frequency. Equation 8 approximates the spectral content of $x[n]$ since it does not consider the samples comprised between two essential samples. In some sense, those samples could be obtained from the essentials which highlights the fact that they are not important. By decreasing the interpolation error, the approach error tends to zero, but increases the number of operations.

Fig. 6 shows the spectrum of a test signal composed of three sinusoids. Observe the high frequency content due to the elimination of the non-essential samples taking zero value for the algorithm.

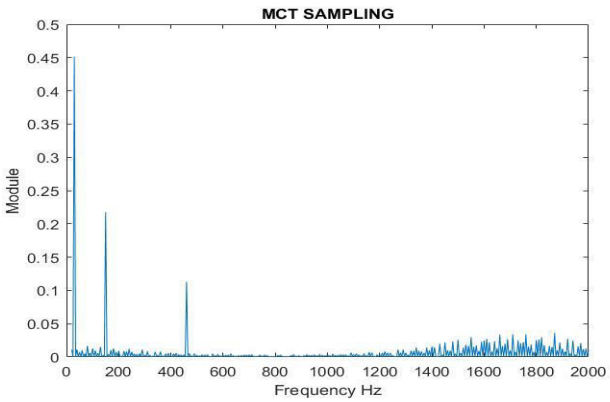

Fig. 6. Spectrum module of a test signal sampled at 4000 Hz using MCT DFT. Note the high frequency content due to the sampling aproximation. Interpolation error 1%.

The efficiency of the DFT MCT compared to the FFT method depends on number of frequency of interest and the interpolation error. For a signal of length N, the number of complex operations in DFT MCT is:

$$H * M \tag{9}$$

While FFT takes:

$$N * log_2 N \tag{10}$$

Where H is number of frequencies of interest and M is the number of essential samples. By evaluating equations (9) and (10), information is obtained to decide on the implementation.

VI. MATLAB SIMULATIONS

Implementing the state-space model in previous section along with the optimal control law, the detailed block diagram in Fig. 7 is obtained.

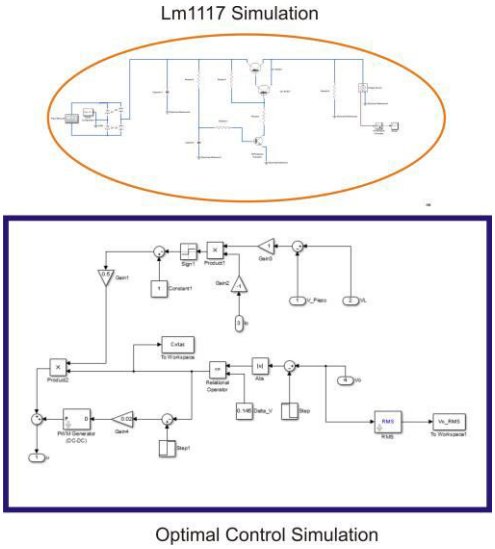

Fig. 7. Optimal control plus lm1117 detail.

VII. Final Implementation: Hardware and Measurements

It turns out that the control law (5) needs the measurement of some internal voltages but, ate the same time, the determination of switching times governed by the sign function.
In [6], this switching function was implemented on-chip using the internal analog-to-digital converters (A/D), however as reported in [13], lower consumptions are obtained when low power Operational Amplifiers (OA) are used.
Moreover, the Texas' microcontroller MSP430G2553 utilized in [6] is now replace by the MSP430G2230 with just the number of input/outputs pins avoiding unused pins.
Finally, the battery-less architecture is achieved if and only if the source for the microcontroller voltage comes from the piezoelectric, and for that, a specialized auto-triggered circuit using an LDO LM1117 was designed.

A. *MSP430G2230 Voltage source uisng LM1117*

The LDO Lm1117 regulates the output voltage about 3.3V to be used for the microcontroller MSP430G2230, whereas the R-C net reset the switching Darlington pair (Fig. 8).

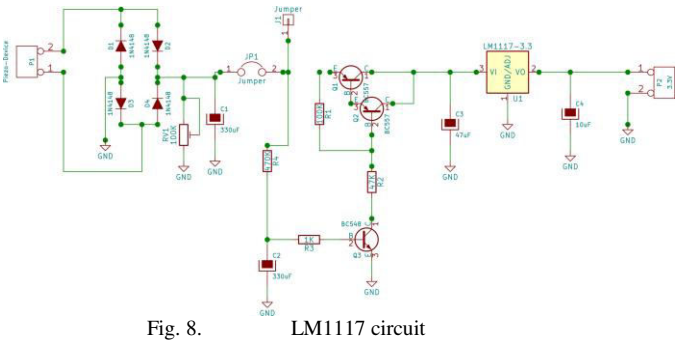

Fig. 8. LM1117 circuit

B. *Optimal Control using Operational Amplifiers OPA333*

As described, the switching optimal control law obtained can be directly implemented using OA rail-to-rail (Fig. 9).

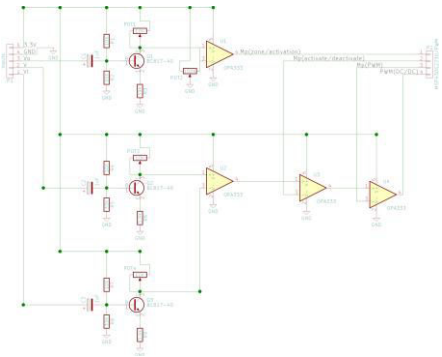

Fig. 9. Analog optimal control's circuit

C. *Feeding a SEEED STUDIO Bluetooth: 100mW*

A final test before implementing the FFT and transmission with a Linksys specialized transmitter (up to 500 m), a low power Bluetooth from SEEED STUDIO was fed with a consumption of about 100mW during 20msecs (Fig. 10 and Fig. 11).

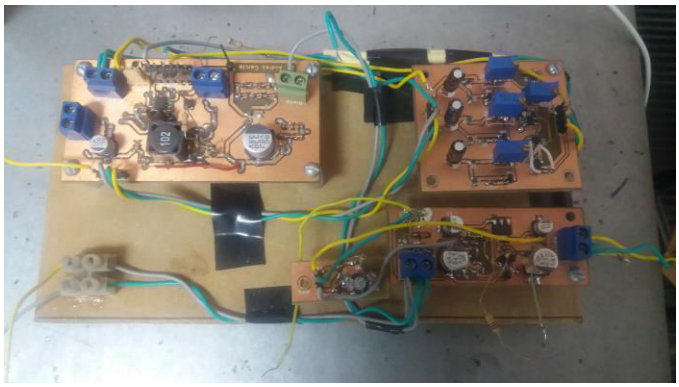

Fig. 10. Complete optimal control

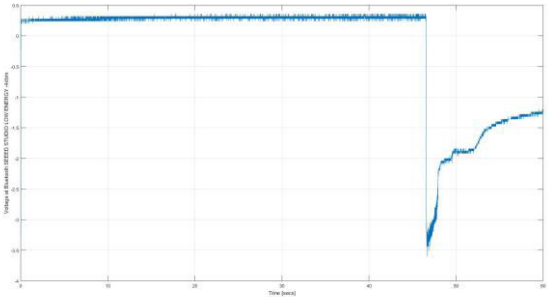

Fig. 11. Bluetooth regulated feeding.

Acknowledgment

The authors would like to acknowledge UTN-FRN, UTN-FRBB, GIMAP under the project ENTUNBB0004269.

VIII. Conclusions

A low power solution to harvest energy from a piezoelectric device in a truly optimal battery-less way was presented.

As a result of a state-space model introduced in [6] with recursion, an optimal cost functional was formulated and solved.

This optimal problem leads a closed-loop control policy using switching sign functions exclusively. This switching function can be implemented naturally using low power operational amplifiers (OPA333).

This implementation reduces the consumption inherently needed to feed the microcontroller (MSP430G2230), thus increasing the amount of energy harvested.

Besides, the novelty implementing an analog control law, some tests were conducted transmitting wireless accelerations from a three axis mems accelerometer and the perform on-chip FFT calculations (using a Cortex M4 STM32L4) allowing for real-time vibration analysis applied to wind energy turbines.

As a future work, improvements using other architectures: Cùk DC-DC and pure LDO solutions are to be studied, as long as other FFT applications such as biomedical sensors in real-time.

REFERENCES

[1] NamAdnan Harb, Energy harvesting: State-ofthe-art, Renewable Energy: Generation and Application, vol.36, issue 10, pp. 2641-2654, 2011

[2] Alperen Toprak and Onur Tigli. Piezoelectric Energy Harvesting: State-Of-The-Art and Challenges. Applied Physics Reviews. vol. 1, issue 3, 2014.

[3] Noha Aboulfotoh, Jens Twiefel. On developing an optimal design procedure for a bimorph piezoelectric cantilever energy harvester under a predefined volume, Mechanical Systems and Signal Processing, vol. 106, pp. 1-12, 2018.

[4] K.Viswanath Allamraju K.Srikanth. State of art: Piezoelectric Vibration Energy Harvesters, Materials Today: Proceedings, vol. 4, issue 2, Part A, pp. 1091-1098, 2017.

[5] Alper Erturk and Daniel J. Inman. Piezoelectric Energy Harvesting. John Wiley & Sons, Ltd. March 2011

[6] A. García, L: Pons and E. Perotti. On the Internal Structure of Piezo-Electric Devices: Closed and Open Loop Optimal Strategies. WSEAS Transactions on Circuits and Systems, vol.16, pp. 196-204, 2017.

[7] Koszewnik, A., Grześ, P. and Walendziuk. Mechanical and electrical impedance matching in a piezoelectric beam for Energy Harvesting. W. Eur. Phys. J. Spec. Top., pp. 224: 2719. 2015.

[8] E. Lefeuvre, D. Audigier, C. Richard and D. Guyomar. *Buck-Boost Converter for Sensorless Power Optimization of Piezoelectric Energy Harvester*. IEEE Transactions on Power Electronics,Vol. 22, Number 5, pp. 2018-2025, 2007.

[9] J. C. Young. Vibration analysis using a mems accelerometer. MSc Electrical Engineering, Naval Postgraduate School, Monterey. 2006.

[10] O. O. ESU, J. A. FLINT and S. J. WATSON. Condition monitoring of

[11] wind turbine blades using MEMS accelerometers. Renewable Energy World Europe (REWE), Vienna, Austria, June 2013.

[12] Peter Spies, Markus Pollak, Loreto Mateu. Handbook of Energy

[13] Harvesting Power Supplies and Applications. June 1, 2015 by Pan Stanford.

[14] Hans P. Geering. Optimal Control with Engineering Applications. Springer, 2007.

[15] Ultra-Low Power Comparison: MSP430 vs. Microchip XLP Tech Brief A Case for Ultra-Low Power Microcontroller Performance. Texas Instruments Report. http://www.ti.com/lit/wp/slay015/slay015.pdf.

[16] YM Lu, MN Do, "A theory for sampling signals from a union of subspaces".Signal Processing, IEEE Transactions on 56 (6), 2334-2345-2008.

[17] G. Monte, "Sensor Signal Preprocessing Techniques for Analysis and Prediction" Industrial Electronics, 2008. IECON 2008. 34th Annual Conference of IEEE. pp 1788-1793. ISBN 978-114244-1766-7.

[18] G. Monte, Z. Liu, F. Abate, V. Paciello, A. Pietrosanto, and V. Huang,"Normalizing transducer signals: An overview of a proposed standard,"in Proceedings IEEE International Instrumentation Measurement Technology Conference (I2MTC), Montevideo, Uruguay, May 2014, pp.614-619.